Supporting Information

High-Nuclearity and Thiol Protected Core-Shell [Cu$_{75}$(S-Adm)$_{32}$]$^{2+}$: Distorted Octahedra Fixed to Cu$_{15}$ Core via Strong Cuprophilic Interactions

Jie Tang[a][f], Chong Liu[b], Chenyu Zhu[a], Keju Sun[c], He Wang[a], Wen Yin[a], Chuting Xu[d], Yang Li[d], Weiguo Wang[d], Li Wang[e], Renan Wu[e], Chao Liu[a], and Jiahui Huang*[a]*

Dalian National Laboratory for Clean Energy, Dalian Institute of Chemical Physics, Chinese Academy of Sciences. Dalian 116023, China; School of Chemical Engineering, Sichuan University. Chengdu 610065, China; College of Environmental and Chemical Engineering, Yanshan University. Qinhuangdao 066004, China; Center for Advanced Mass Spectrometry, Dalian Institute of Chemical Physics, Chinese Academy of Sciences. Dalian 116023, China; Laboratory of High-Resolution Mass Spectrometry Technologies, CAS Key Laboratory of Separation Science for Analytical Chemistry, Dalian Institute of Chemical Physics, Chinese Academy of Sciences. Dalian 116023, China; University of Chinese Academy of Sciences. Beijing 100049, China.

*To whom correspondence should be addressed. Email: chaoliu@dicp.ac.cn

Notes: The authors declare no competing financial interest.

Supplementary Tables

Table S1. Crystal data and structure refinement for **Cu₇₅** nanocluster.

Empirical formula	$C_{320}H_{480}Cu_{75}S_{32}$
Formula weight	10118.43
Temperature/K	173.0
Crystal system	triclinic
Space group	P-1
a/Å	23.6279(5)
b/Å	23.6779(5)
c/Å	23.8819(5)
α/°	112.1310(10)
β/°	119.5380(10)
γ/°	92.9240(10)
Volume/Å³	10292.9(4)
Z	1
$\rho_{calc}g/cm^3$	1.632
μ/mm^{-1}	5.813
F(000)	5087.0
Crystal size/mm³	0.1 × 0.1 × 0.1
Radiation	CuKα (λ = 1.54178)
2Θ range for data collection/°	4.214 to 124.77
Index ranges	-27 ≤ h ≤ 27, -24 ≤ k ≤ 27, -27 ≤ l ≤ 27
Reflections collected	93609
Independent reflections	31471 [R_{int} = 0.1040, R_{sigma} = 0.1068]
Data/restraints/parameters	31471/402/1828
Goodness-of-fit on F^2	1.594
Final R indexes [I>=2σ (I)]	R_1 = 0.1854, wR_2 = 0.4530
Final R indexes [all data]	R_1 = 0.2510, wR_2 = 0.5012
Largest diff. peak/hole / e Å⁻³	4.50/-2.00

Table S2. Selected Cu-Cu bond lengths (Å) of **Cu$_{75}$** nanocluster.

Anchor–Core	Bond length	Anchor–Vertex	Bond length
Cu26-Cu24	2.430(6)	Cu18-Cu38	2.715(6)
Cu26-Cu4	2.401(7)	Cu18-Cu20	2.501(9)
Cu33-Cu37	2.393(7)	Cu12-Cu23	2.472(4)
Cu12-Cu24	2.38(1)	Cu12-Cu11	2.698(8)
Cu18-Cu25	2.38(1)	Cu26-Cu8	2.552(7)
Cu18-Cu37	2.378(7)	Cu33-Cu34	2.559(6)
Cu33-Cu24	2.36(1)	Cu5-Cu2	2.732(7)
Cu35-Cu31	2.357(6)	Cu12-Cu14	2.50(1)
Cu5-Cu21	2.352(6)	Cu5-Cu16	2.529(5)
Cu12-Cu21	2.347(8)	Cu33-Cu32	2.522(8)
Cu5-Cu4	2.344(6)	Cu18-Cu19	2.452(6)
Cu26-Cu25	2.341(9)	Cu26-Cu9	2.492(8)
Cu12-Cu17	2.340(6)	Cu5-Cu6	2.524(6)
Cu35-Cu4	2.339(8)	Cu26-Cu3	2.452(6)
Cu18-Cu17	2.336(4)	Cu33-Cu10	2.483(8)
Cu35-Cu17	2.330(7)	Cu35-Cu1	2.823(6)
Cu5-Cu37	2.315(8)	Cu35-Cu28	2.479(7)
Cu33-Cu31	2.292(4)	Cu35-Cu29	2.498(8)
Centered–face centered	**Bond length**	**Core–Core**	**Bond length**
Cu13-Cu17	2.728(7)	Cu37-Cu25	2.674(7)
Cu13-Cu25	2.667(9)	Cu37-Cu21	2.671(9)
Cu15-Cu21	2.649(9)	Cu17-Cu21	2.702(8)
Cu15-Cu17	2.684(4)	Cu17-Cu31	2.810(8)
Cu30-Cu17	2.809(7)	Cu24-Cu25	2.745(8)
Cu30-Cu31	2.679(9)	Cu24-Cu31	2.59(1)
Cu26-Cu27	2.170(7)	Cu36-Cu21	2.322
Cu12-Cu15	2.262(7)	Cu36-Cu25	2.335
Cu18-Cu13	2.187(6)	Cu36-Cu31	2.334
Cu5-Cu7	2.166(7)	Cu4-Cu21	2.794(8)
Cu33-Cu22	2.190(6)	Cu4-Cu25	2.68(1)
Cu35-Cu30	2.240(6)	Cu4-Cu31	2.693(6)

Table S3. Selected Cu-S bond lengths (Å) of **Cu$_{75}$** nanocluster.

Cu-Linking μ³-S	Bond length	Cu-Linking μ³-S	Bond length
Cu1-S1	2.249(9)	Cu14-S11	2.208(9)
Cu2-S1	2.193(9)	Cu20-S11	2.175(6)
Cu3-S1	2.167(8)	Cu29-S11	2.181(8)
Cu16-S4	2.351(8)	Cu10-S12	2.16(1)
Cu22-S4	2.174(8)	Cu11-S12	2.32(1)
Cu23-S4	2.150(9)	Cu9-S12	2.185(7)
Cu30-S6	2.172(7)	Cu11-S13	2.341(7)
Cu32-S6	2.44(1)	Cu13-S13	2.184(9)
Cu38-S6	2.369(9)	Cu8-S13	2.38(1)
Cu27-S7	2.18(1)	Cu19-S15	2.19(1)
Cu28-S7	2.145(7)	Cu7-S15	2.20(1)
Cu32-S7	2.284(6)	Cu8-S15	2.289(7)
Cu1-S10	2.462(9)	Cu34-S16	2.215(9)
Cu15-S10	2.149(7)	Cu38-S16	2.265(8)
Cu16-S10	2.36(1)	Cu6-S16	2.19(1)
Cu-Top μ³-S	**Bond length**	**Cu-Top μ³-S**	**Bond length**
Cu16-S2	2.319(8)	Cu1-S8	2.29(1)
Cu2-S2	2.204(7)	Cu28-S8	2.187(8)
Cu6-S2	2.300(9)	Cu29-S8	2.263(8)
Cu11-S3	2.42(1)	Cu19-S9	2.20(1)
Cu14-S3	2.383(7)	Cu20-S9	2.269(7)
Cu23-S3	2.18(1)	Cu38-S9	2.34(1)
Cu10-S5	2.43(1)	Cu3-S14	2.47(1)
Cu32-S5	2.282(6)	Cu8-S14	2.34(1)
Cu34-S5	2.339(9)	Cu9-S14	2.432(9)

Table S4. Cu-S-Cu angles (°) of **Cu$_{75}$** nanocluster.

Vertex -Top μ³-S-vertex	Angles (°)	Vertex -linking μ³-S-vertex	Angles (°)
Cu38-S9-Cu19	77.8(4)	Cu23-S4-Cu16	110.4
Cu19-S9-Cu20	88.2(4)	Cu16-S4-Cu22	98.2
Cu20-S9-Cu38	88.4(4)	Cu22-S4-Cu23	93.3
Cu29-S8-Cu28	85.1(3)	Cu34-S16-Cu6	103.6
Cu28-S8-Cu1	79.6(3)	Cu6-S16-Cu38	123.9
Cu1-S8-Cu29	93.6(3)	Cu38-S16-Cu34	89.3
Cu32-S5-Cu34	75.8(3)	Cu8-S15-Cu7	99.8
Cu34-S5-Cu10	93.0(3)	Cu7-S15-Cu19	90.2
Cu10-S5-Cu32	78.4(3)	Cu8-S15-Cu19	110.4
Cu11-S3-Cu23	81.5(3)	Cu1-S10-Cu16	121.8
Cu23-S3-Cu14	83.5(3)	Cu16-S10-Cu15	87.9
Cu11-S3-Cu14	85.7(3)	Cu15-S10-Cu1	102.6
Cu2-S2-Cu16	77.1(3)	Cu2-S1-Cu3	103
Cu2-S2-Cu6	100.0(3)	Cu3-S1-Cu1	117.9
Cu6-S2-Cu16	80.3(3)	Cu1-S1-Cu2	93.5
Cu3-S14-Cu9	91.5(3)		
Cu9-S14-Cu8	74.1(3)		
Cu8-S14-Cu3	79.1(3)		

Supplementary Figures
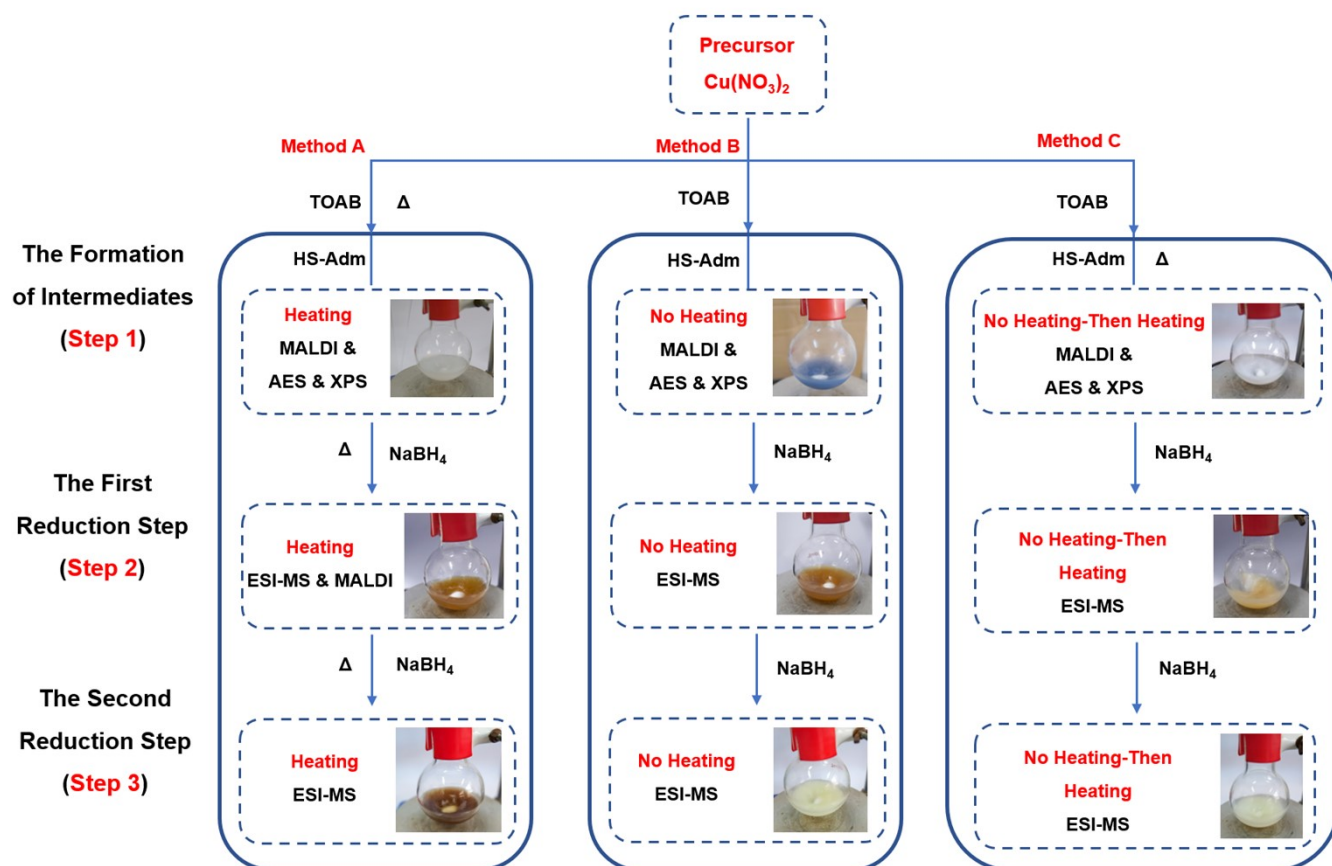
Scheme S1. The standard method of the preparation of Cu$_{75}$ (Method A), the same procedure but without heating steps (Method B), and the solution was heated up after the addition of Ligands (Method C). More details are provided in the Materials and methods.
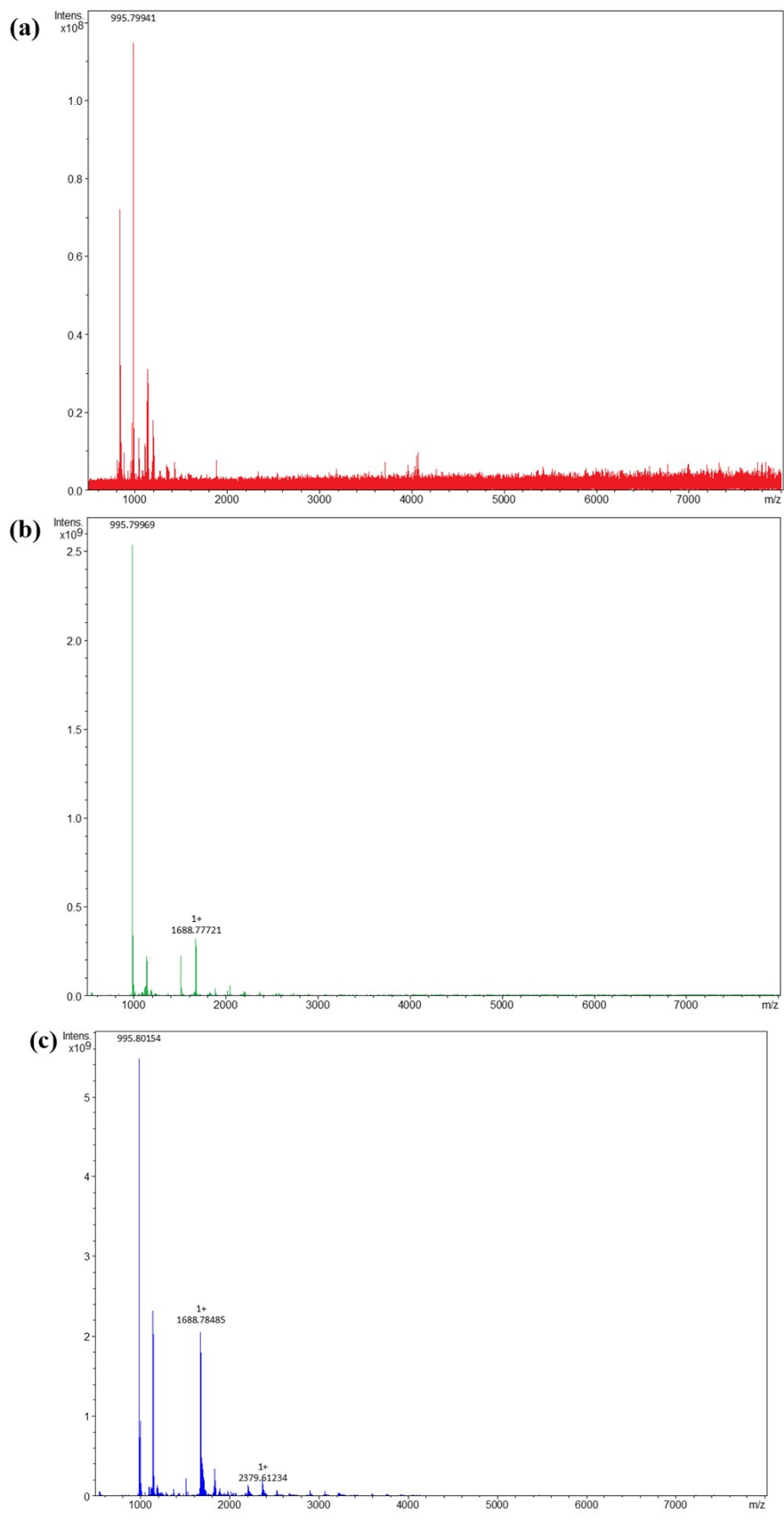
Fig. S1 The MALDI analysis of the sediments obtained in Step 1 in (a) Method A (Cu_{75}), (b) Method B and (c) Method C.
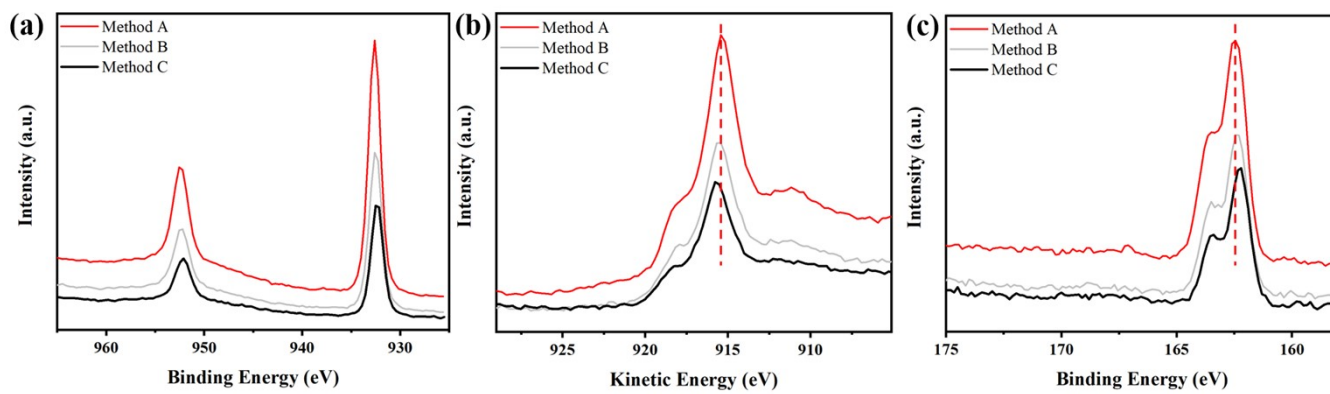
Fig. S2 The XPS and AES analysis of the sediments obtained in the Step 1 in the three methods. (a) High-resolution XPS spectra of Cu 2p, (b) LMM Auger spectrum of Cu, and (c) High-resolution XPS spectra of S 2s.
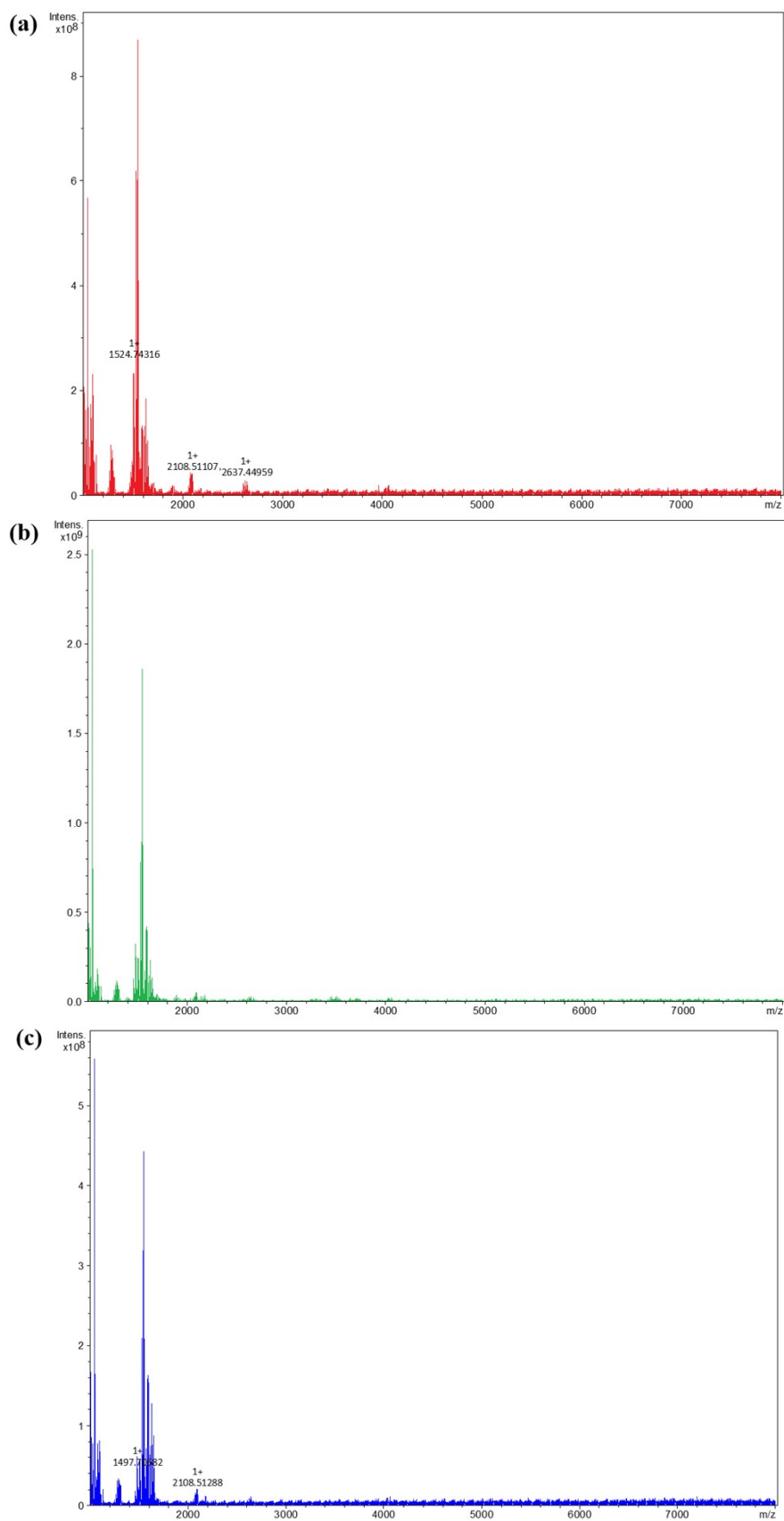
Fig. S3 The ESI-MS analysis of supernate obtained in the Step 2 in (a) Method A (Cu_{75}) (b) Method B and (c) Method C.
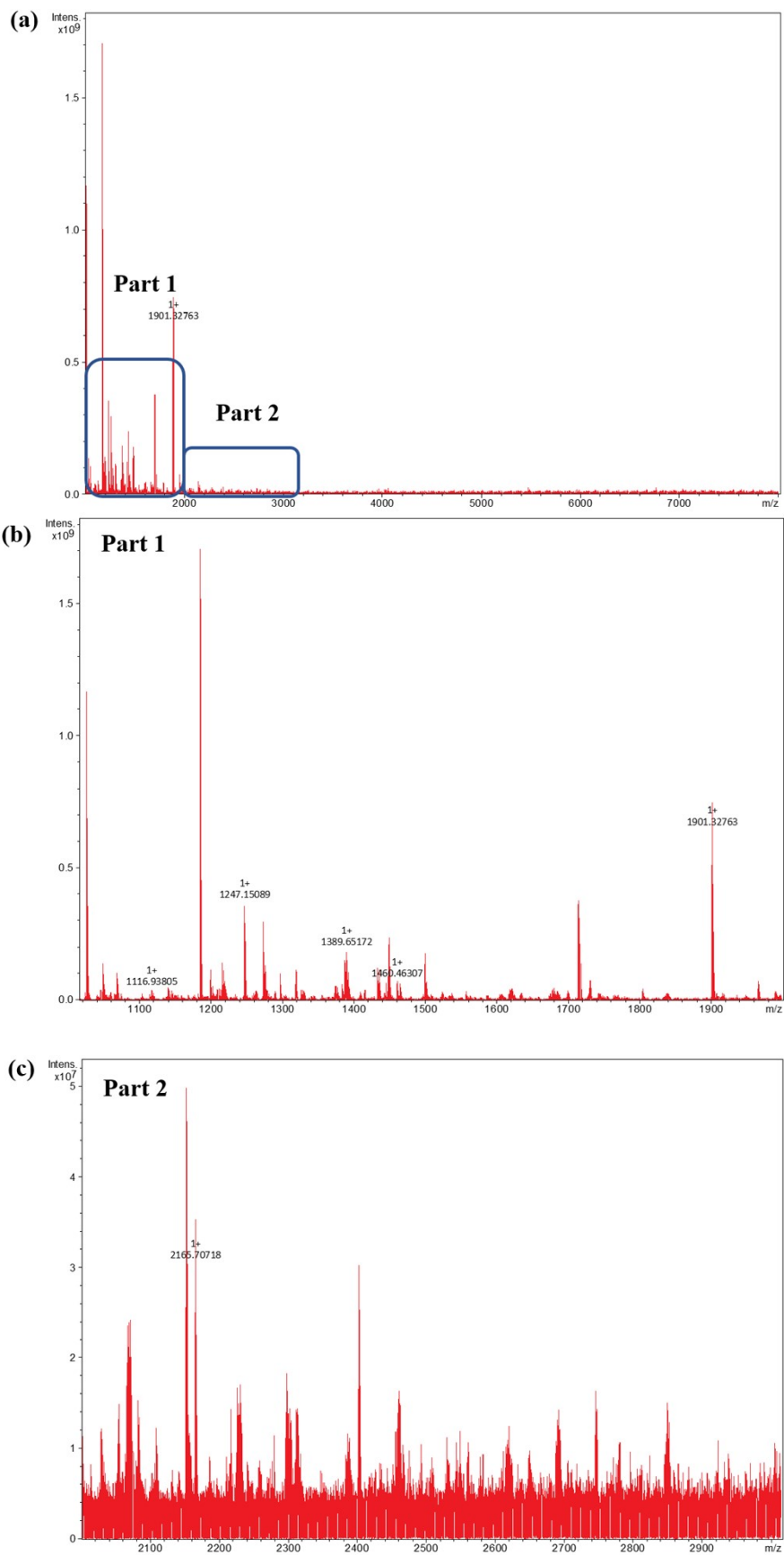
Fig. S4 The MALDI analysis of Sediments obtained in the Step 2 in Method A (Cu_{75}). (a) The overall analysis of sediments, (b) the detailed part 1 in sediments and (c) the detailed part 2 in sediments.
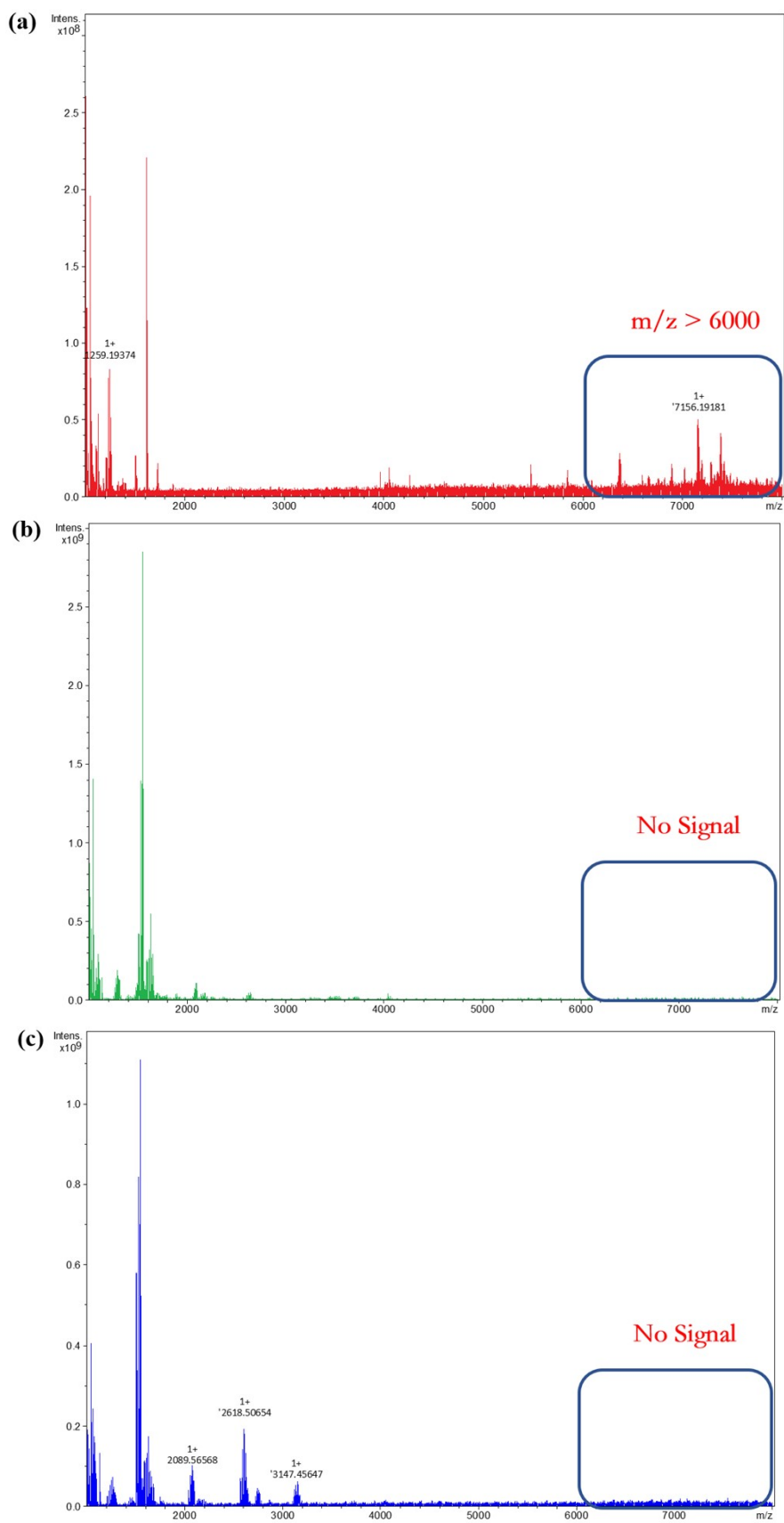
Fig. S5 The ESI-MS analysis of Sediments obtained the Step 3 in solution of (a) Method A (Cu_{75}), (b) Method B and (c) Method C.
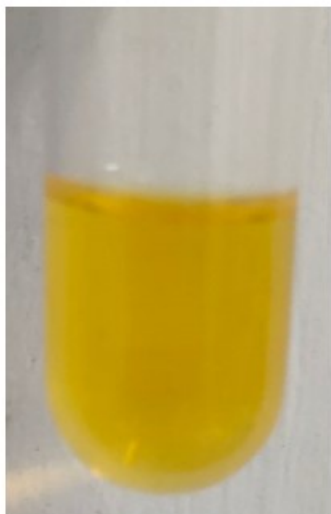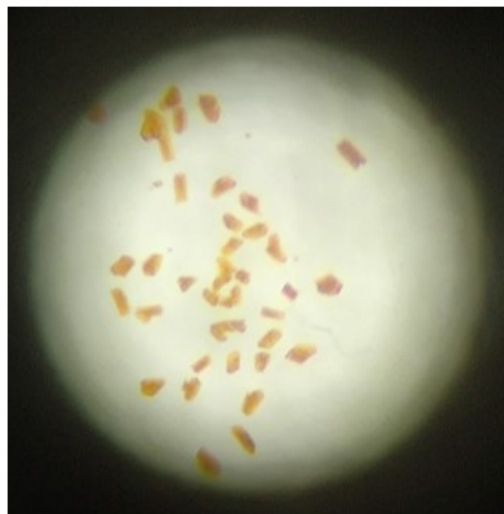
Fig. S6 A representative optical microscopic image of a) solution and b) single crystals of **Cu$_{75}$** nanocluster.
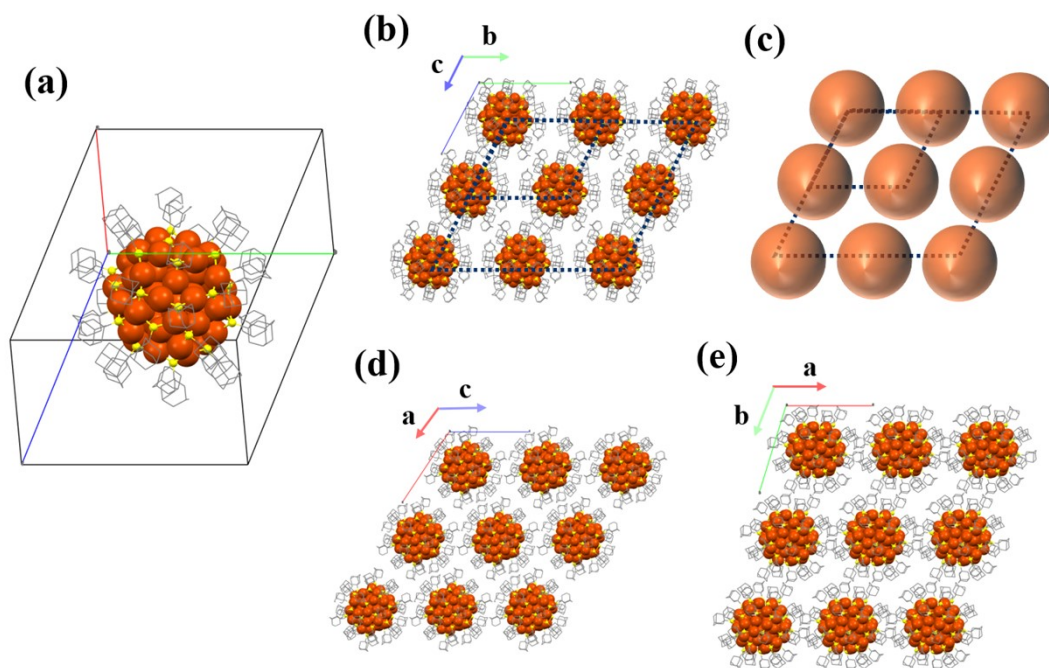
Fig. S7 Cu$_{75}$ in a single unit cell (a). Different views of the packing fashion of **Cu$_{75}$** along a axis (b), b axis (d) and c axis (e). Diagram of orderly arranged **Cu$_{75}$** nanocluster packing mode (c).
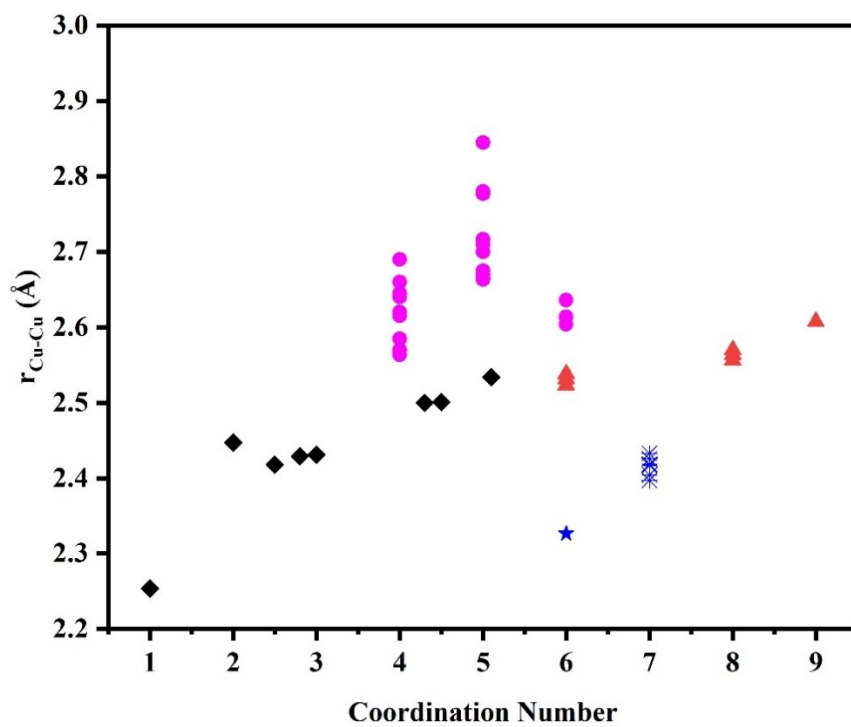
Fig. S8 The relationship between coordination number and average $r_{Cu\text{-}Cu}$. Black rhombus (◆): computational data of Cu clusters (Cu_2-Cu_9). Pink dot (●): Cu-shell-vertex. Red triangle (▲): Cu-core-anchor. Blue snowflake (✳): Cu-core. Bule star (★): centered Cu-core.
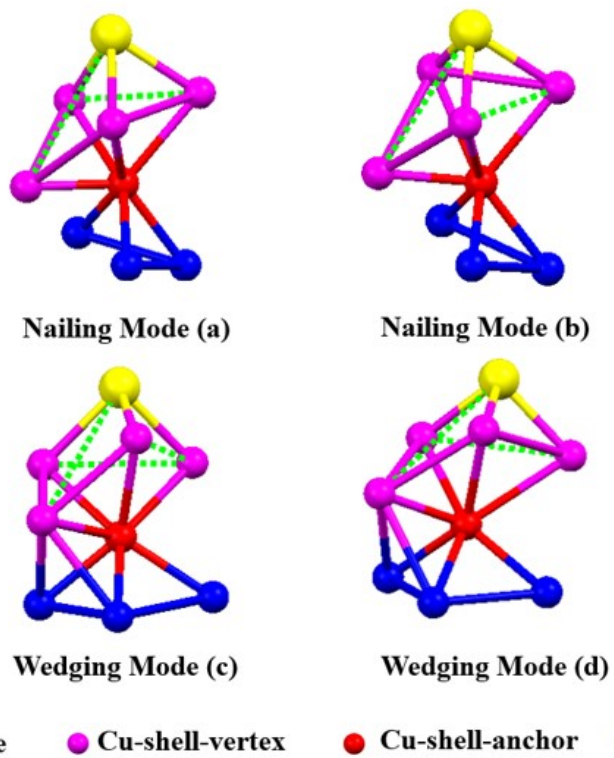
Fig. S9 Four kinds of different bonding modes (a, b, c, d) between distorted octahedrons of shell and centered face-centered cubic of core.
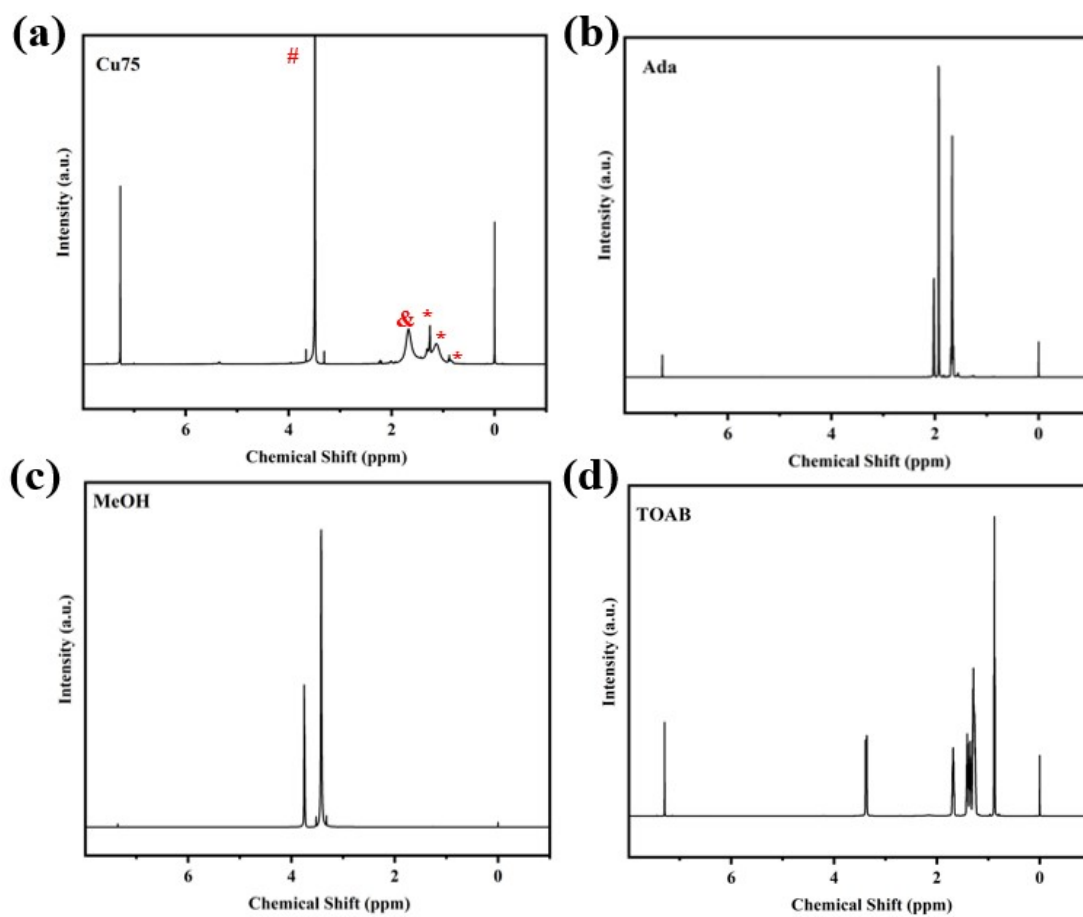
Fig. S10 ^{1}H NMR (CDCl$_3$, 700 MHz) spectra of **Cu$_{75}$** nanocluster (a), free 1-Ada (b), MeOH (c) and TOAB (d). The marked peaks correspond to methanol (#), HS-Adm (&) and impurities (*).
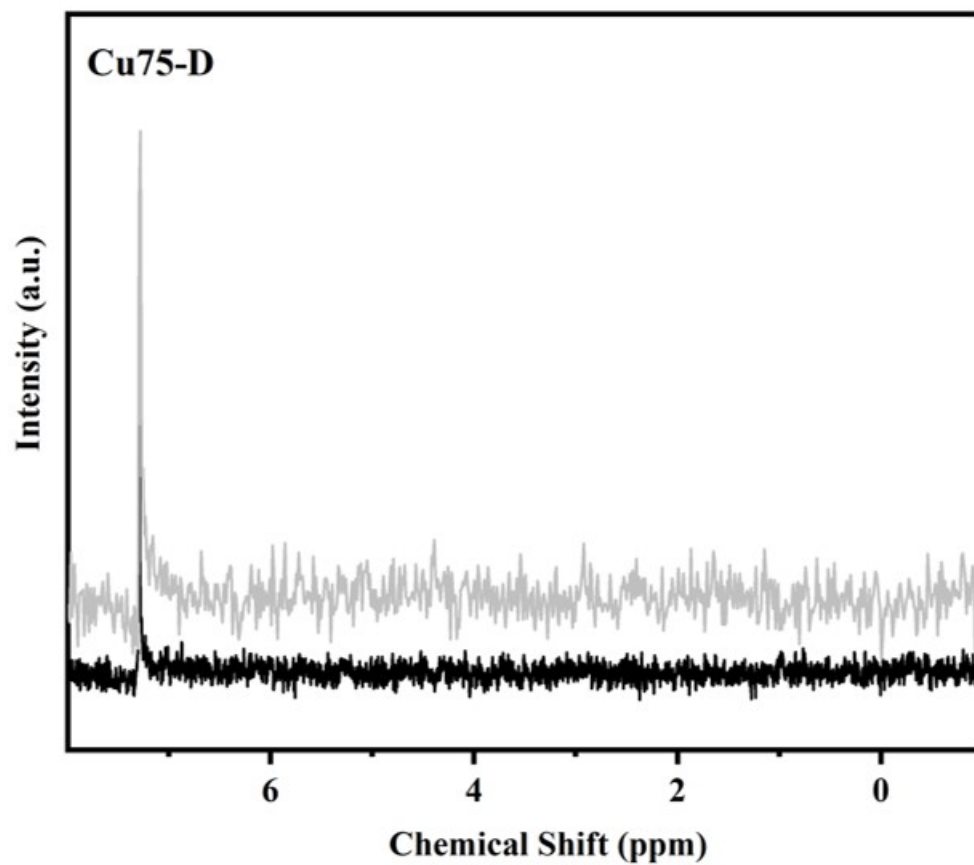
Fig. S11 Two times of experiments of ^{1}D NMR (CHCl$_3$, 700MHz) spectra of **Cu$_{75}$-D** for insurance of no D in **Cu$_{75}$-D**.
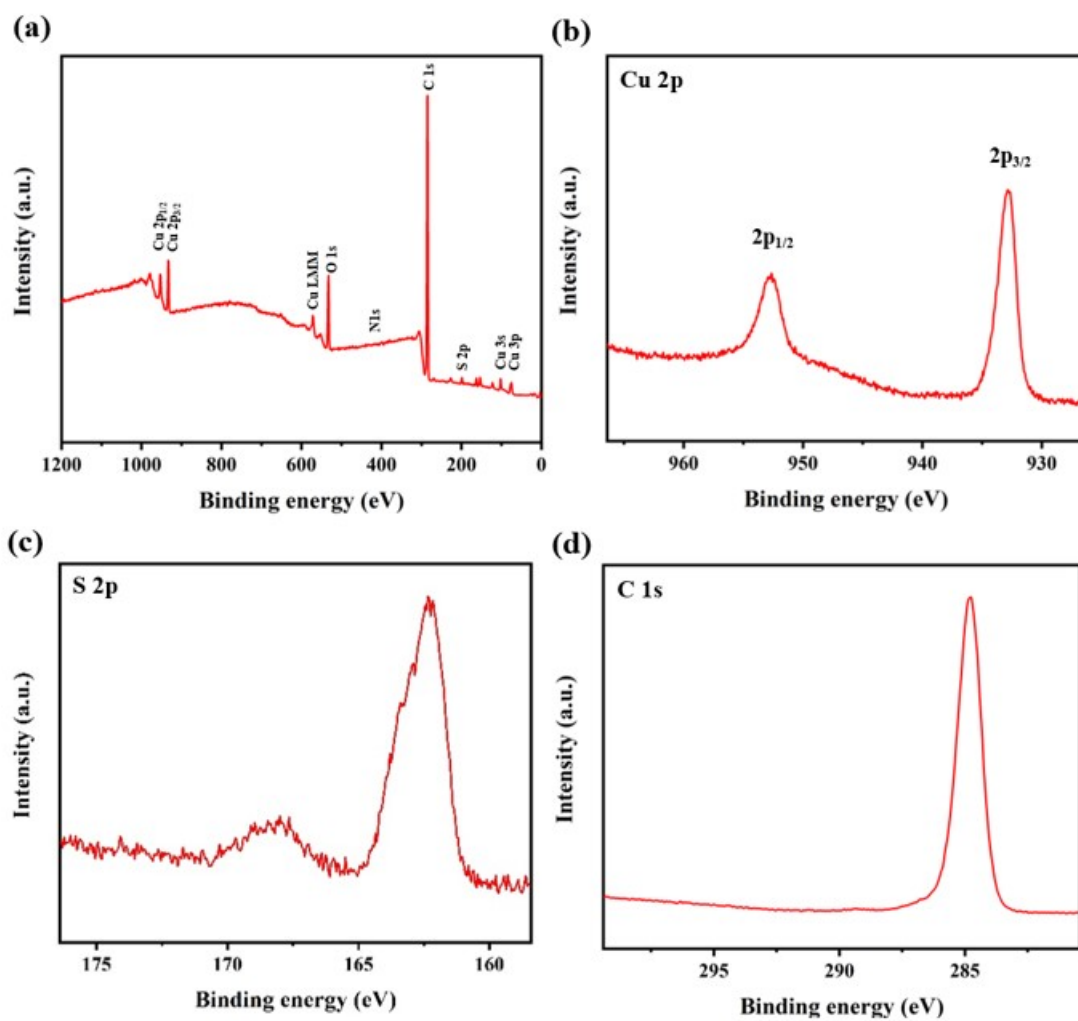
Fig. S12 (a) The full XPS spectrum of **Cu₇₅** nanocluster. High-resolution XPS spectra of Cu 2p (b), S 2p (c), C 1s (d).
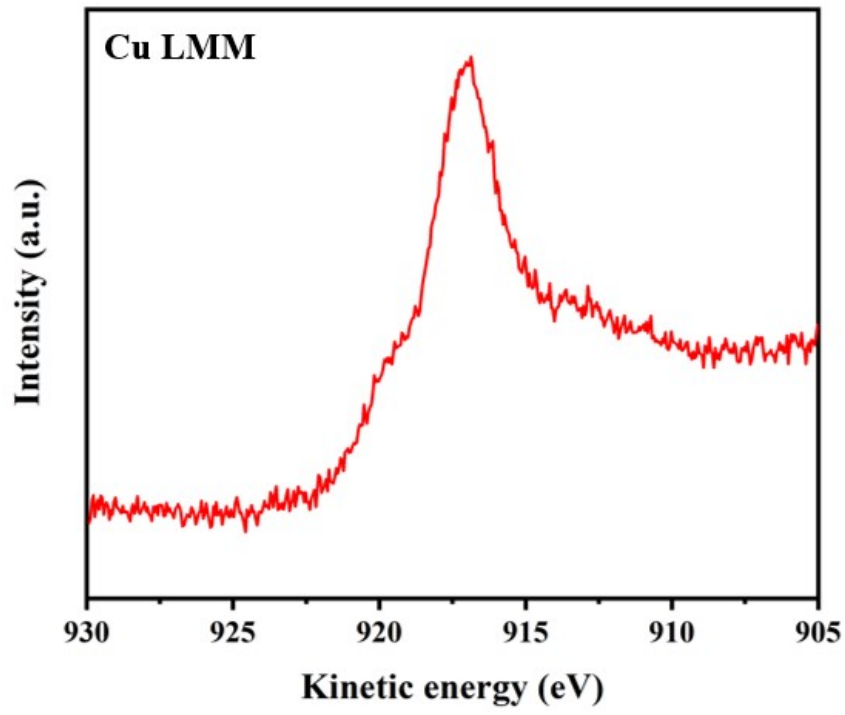
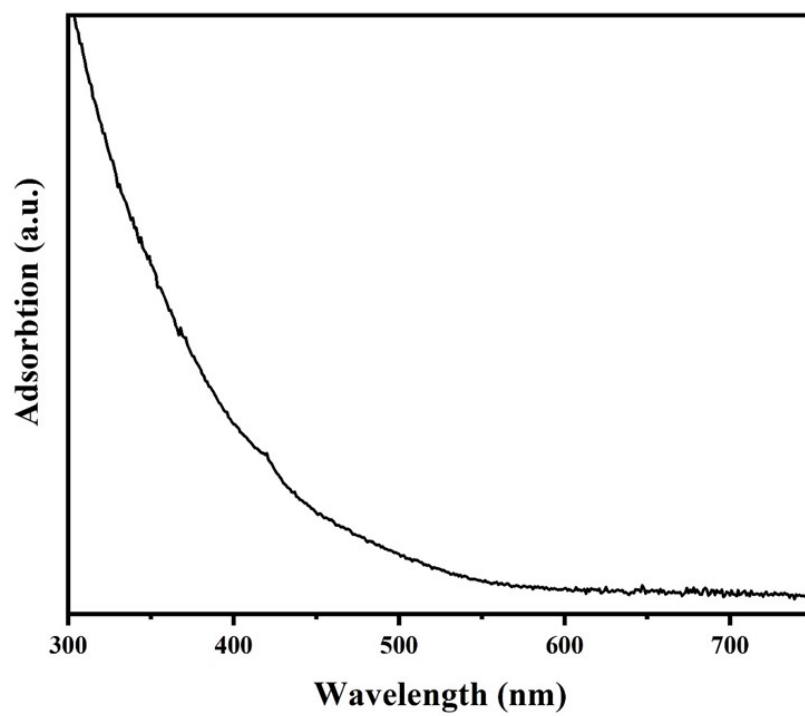**Fig. S13** Cu LMM Auger spectrum of **Cu₇₅** nanocluster.

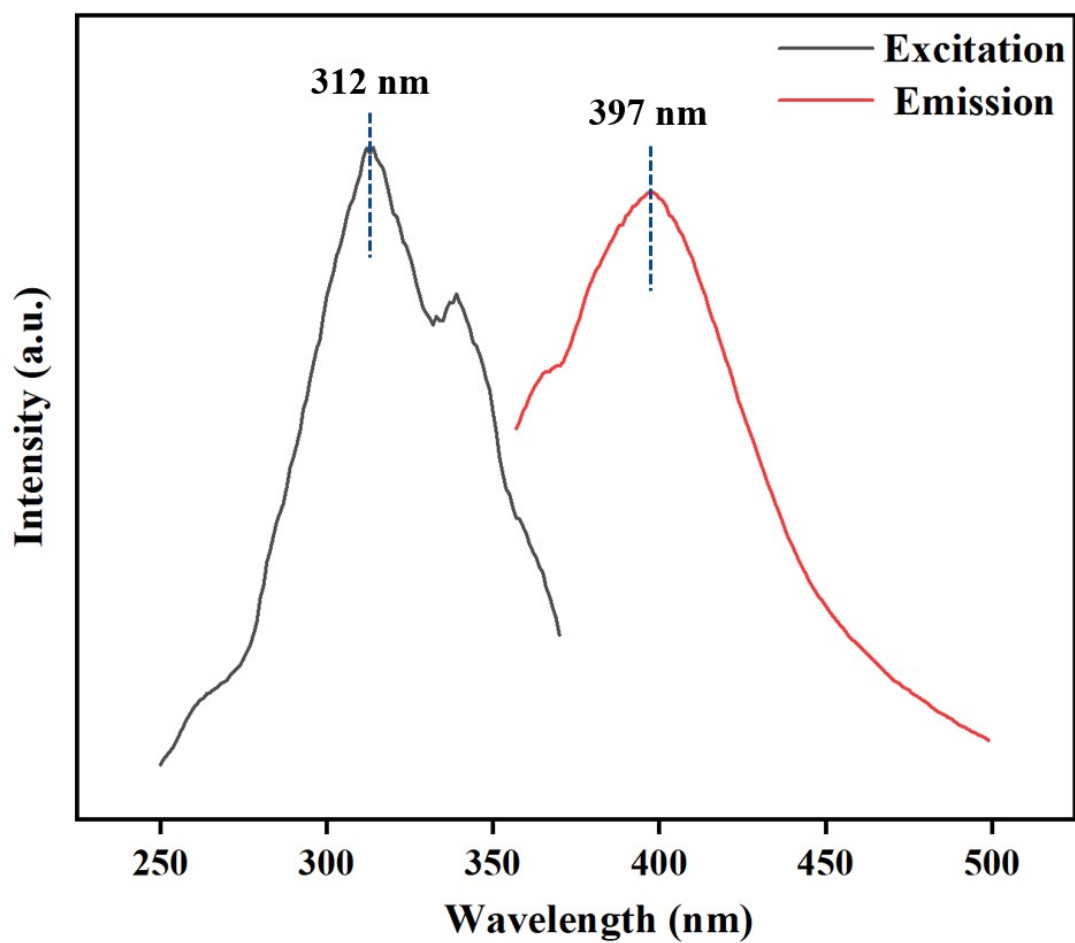**Fig. S14** The Uv-vis spectrum of **Cu₇₅** crystals dissolved in toluene.

Fig. S15 Steady-state excitation (black) and emission (red) spectra of the **Cu$_{75}$** in toluene.
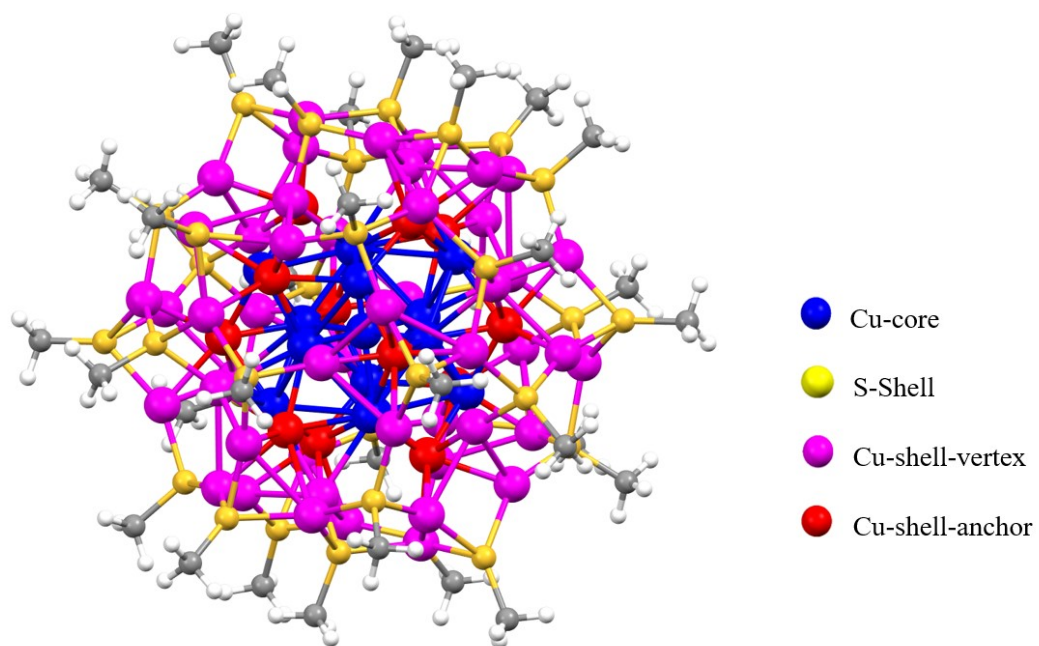
Fig. S16 The DFT calculation model of **Cu$_{75}$(S-CH$_3$)$_{32}$** nanocluster.

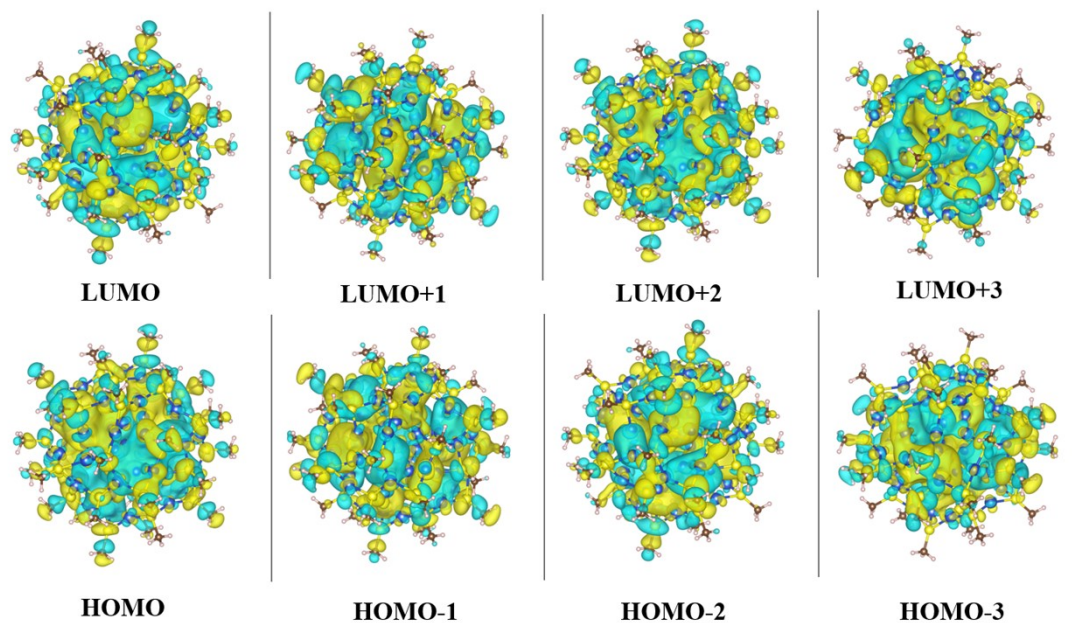|			
LUMO	**LUMO+1**	**LUMO+2**	**LUMO+3**
HOMO	**HOMO-1**	**HOMO-2**	**HOMO-3**

Fig. S17 DFT calculations of corresponding electronic charge densities of the **Cu$_{75}$(S-CH$_3$)$_{32}$** nanocluster for HOMO-3 to LUMO+3.